LETTERS

Observation of spin-dependent quantum jumps via quantum dot resonance fluorescence

A. N. Vamivakas[1]*, C.-Y. Lu[1,2]*, C. Matthiesen[1]*, Y. Zhao[1,3], S. Fält[4], A. Badolato[5] & M. Atatüre[1]

Reliable preparation, manipulation and measurement protocols are necessary to exploit a physical system as a quantum bit[1]. Spins in optically active quantum dots offer one potential realization[2,3] and recent demonstrations have shown high-fidelity preparation[4,5] and ultrafast coherent manipulation[6–8]. The final challenge—that is, single-shot measurement of the electron spin—has proved to be the most difficult of the three and so far only time-averaged optical measurements have been reported[9–12]. The main obstacle to optical spin readout in single quantum dots is that the same laser that probes the spin state also flips the spin being measured. Here, by using a gate-controlled quantum dot molecule[13–15], we present the ability to measure the spin state of a single electron in real time via the intermittency of quantum dot resonance fluorescence[12,16]. The quantum dot molecule, unlike its single quantum dot counterpart, allows separate and independent optical transitions for state preparation, manipulation and measurement, avoiding the dilemma of relying on the same transition to address the spin state of an electron.

The concept of using resonance fluorescence (RF) to probe internal atomic state dynamics dates from 1975 (ref. 17) with the first demonstrations from trapped ions in 1986 (refs 18–20) followed by single molecules[21]. Since then RF has become the state measurement technique in ion-based quantum information processing[22]. Analogously it was proposed that RF from a single quantum dot (QD) trion (charged exciton) transition would reveal the spin state of an electron[23,24]. A physical constraint to observing real-time spin quantum jumps in the RF from a resonantly driven QD trion transition is that the timescale for the measurement laser to induce a spin flip (useful for state preparation[4,5]) must be longer than the timescale to complete a reliable measurement. The heavy–light hole mixing and the external magnetic field orientation with respect to the QD growth axis constrain the measurement timescale to at most a few microseconds[25,26]. This leads to a preparation–measurement dilemma in which fast preparation[8] and reliable measurement of an electron spin cannot be simultaneously realized.

One remedy is to decouple the spin preparation and measurement transitions by using a QD molecule consisting of two vertically stacked indium arsenide QDs in gallium arsenide embedded in a Schottky diode heterostructure[13–15] (see Fig. 1a and Methods). We operate in a gate voltage regime where the QD closest to the electron reservoir (host QD) is single-electron charged while the other (readout) QD remains empty. The ground and excited QD molecule states relevant for our work are illustrated in Fig. 1b (ref. 27). The ground (0, 1) and excited ($S_{\pm 3/2}$) states of the host QD are identical to those of a single QD and these transitions are used for spin state preparation (write-in). The QD molecule also supports distributed trion states consisting of an electron in the host QD and an exciton in the readout QD. This is the only charge configuration that exhibits electronic tunnel coupling. Under a finite magnetic field along the QD molecule growth direction, spin-dependent interactions lift the degeneracy of the 12 molecular states of this configuration[27–29] (see Supplementary Information) and each state becomes spectrally addressable. The essential state for this work in Fig. 1b is $T_{+1/2}$. Optical excitation to the $T_{+1/2}$ state is possible only when the host QD electron is in state 1 and our approach to readout relies on monitoring the intermittent RF from the 1-to-$T_{+1/2}$ transition.

To demonstrate that the 1-to-$T_{+1/2}$ transition is conditional on the host QD electron spin we performed time-averaged two-colour RF

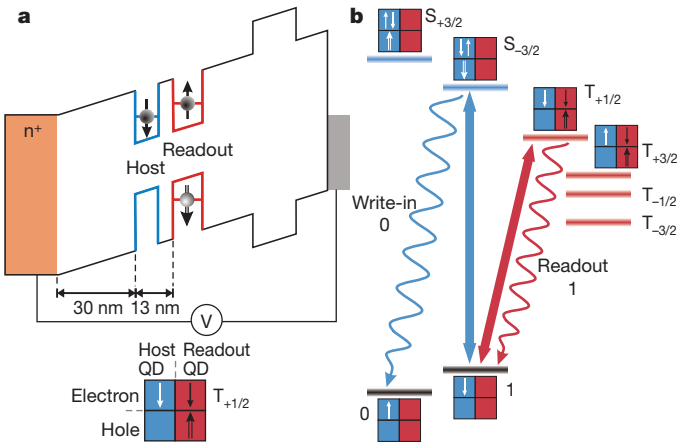

Figure 1 | Sample structure and quantum dot molecule transition diagram. **a**, The quantum dot molecule consists of two vertically stacked indium arsenide QDs in gallium arsenide. The host QD is 30 nm above the n-doped layer (n+) and the readout QD wetting layer is separated from the host QD wetting layer by 13 nm. The inset in **a** defines our notation used in **b**: to describe the permissible spin configurations we use a box in which the left column refers to the host QD and the right column to the readout QD. The top row denotes electron spin projections (single line arrow) and the bottom row hole spin projections (double line arrow). In the inset illustration the spin configuration corresponds to the molecular trion triplet labelled $T_{+1/2}$. The value of the subscript is determined from summing the spin projection of each electron and hole ($-1/2-1/2+3/2=+1/2$). **b**, An illustration of the ground and excited states relevant for spin readout via resonance fluorescence with an externally applied magnetic field along the growth direction. The ground state consists of a single electron in the host QD with spin projection $-1/2$ (or $+1/2$), split by the Zeeman energy, which we denote 1 (or, corresponding to spin projection $+1/2$, 0). The two Zeeman-split trion states localized in the host QD are labelled $S_{+3/2}$ and $S_{-3/2}$. Optical pumping on the host QD transitions makes the initialization of the ground state spin to 0 (illustrated) or 1 (not shown) possible. A linearly polarized laser drives the 1-to-$T_{+1/2}$ transition for optical readout.

[1]Cavendish Laboratory, University of Cambridge, JJ Thomson Avenue, Cambridge CB3 0HE, UK. [2]HFNL & Department of Modern Physics, University of Science and Technology of China, Hefei, 230026, China. [3]Physikalisches Institut, Ruprecht-Karls-Universität Heidelberg, Philosophenweg 12, 69120 Heidelberg, Germany. [4]Sol Voltaics AB, Scheelevägen 17, Ideon Science Park, 223 70 Lund, Sweden. [5]Department of Physics and Astronomy, University of Rochester, Rochester, New York 14627, USA.
*These authors contributed equally to this work.

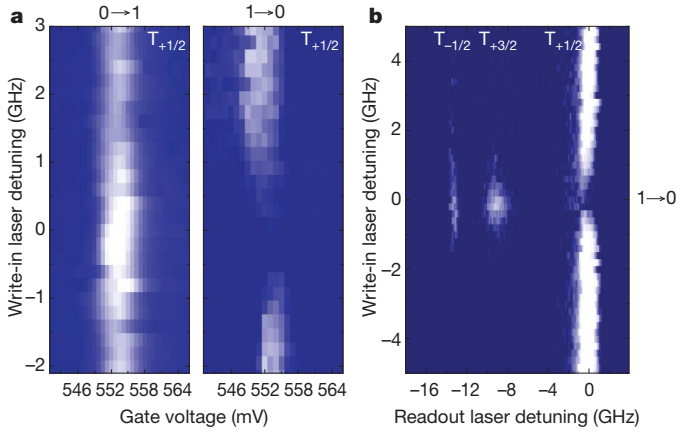

Figure 2 | Steady-state two-colour resonance fluorescence. a, The readout laser frequency is fixed in the vicinity of the 1-to-$T_{+1/2}$ transition at a magnetic field of 2.3 T in the Faraday configuration. The write-in laser frequency is scanned for each gate voltage value and the RF from the readout transition is monitored. White denotes high RF signal and blue is background. Left panel, when the write-in laser prepares the ground state to 1 via optical pumping the readout signal is enhanced. Right panel, when the write-in laser prepares the ground state to 0 the readout signal is suppressed. **b**, At fixed gate voltage both the write-in and readout laser frequencies are scanned. When the write-in laser prepares state 0, extinguishing the RF signal for the 1-to-$T_{+1/2}$ transition, the 0-to-$T_{+3/2}$ and 0-to-$T_{-1/2}$ transitions are enhanced, exhibiting the direct correlation between these transitions and the electron spin.

measurements at a magnetic field of 2.3 T (see Supplementary Information for QD molecule spectroscopy). In the left panel of Fig. 2a the readout laser is fixed in the vicinity of the 1-to-$T_{+1/2}$ transition and for each gate voltage value (the gate voltage Stark-shifts the QD molecule energy levels; see Methods), the write-in laser frequency is scanned across the host QD 0-to-$S_{+3/2}$ transition. The right panel of Fig. 2a shows when the write-in laser frequency is scanned across the 1-to-$S_{-3/2}$ transition. For the double resonance condition, in which the readout laser is resonant with the 1-to-$T_{+1/2}$ transition and the write-in laser prepares state 1, the RF from the 1-to-$T_{+1/2}$ transition is enhanced. Similarly, when the write-in laser prepares state 0, the RF is suppressed. When the electron is in state 0, the $T_{+3/2}$ and $T_{-1/2}$ states are optically accessible, as is evident in Fig. 2b. Here the readout laser frequency is scanned across the $T_{+1/2}$, $T_{+3/2}$ and $T_{-1/2}$ state transitions. When the write-in laser is resonant with the 1-to-$S_{-3/2}$ transition, RF is suppressed on the state-1 readout channel ($T_{+1/2}$), but enhanced on the state-0 transitions ($T_{+3/2}$ and $T_{-1/2}$), confirming the spin conditionality of these transitions. Further, when the write-in laser is detuned from the 1-to-$S_{-3/2}$ transition resonance, the RF signal is suppressed on the 0-to-$T_{+3/2}$ and 0-to-$T_{-1/2}$ transitions. This indicates that, unlike the 1-to-$T_{+1/2}$ transition, these transitions exhibit optical pumping, similarly to a single QD (ref. 30, and see Supplementary Information).

Having identified the 1-to-$T_{+1/2}$ transition as a suitable readout channel, we demonstrate real-time optical monitoring of the host QD spin state as manifested by the intermittency of RF from this transition. The RF photocounts in Fig. 3a, recorded in 250-μs time bins, display telegraph-like switching between 1- and 0-levels for negative time and are quenched for positive time when the host QD spin is prepared in state 0. Figure 3b presents histograms of the 1-to-$T_{+1/2}$ transition RF photocounts for two cases: The first case (red histogram) is obtained when the readout laser drives the 1-to-$T_{+1/2}$ transition. The second case (blue histogram) is obtained when the 1-to-$T_{+1/2}$ transition is driven while the host QD spin is prepared in the 1 state by the write-in laser. Both histograms are obtained from 100-s-long time traces in 4-ms time bins. The regions outlined by the rectangles are displayed in the left panels of Fig. 3b. The summation of RF photocounts below the threshold, indicated by the vertical dashed black line in each of the left panels of Fig. 3b, reveals a nearly threefold suppression when the faint write-in-1 laser is present (at higher laser powers the suppression is more pronounced).

When the electron is in state 1 the readout laser resonantly drives the 1-to-$T_{+1/2}$ transition without optically pumping the spin from state 1 to state 0; however, when the electron is in state 0 the readout laser drives the 0-to-$T_{+3/2}$ transition weakly (owing to 8-GHz spectral detuning), causing a finite spin-flip rate from state 0 to 1. This leads to the unequal peak heights of the two modes in the red histogram of Fig. 3b. To highlight this effect two exemplary off-duration (off is the time when the electron is in state 0) histograms are presented in Fig. 3c for a 1,200-s time trace. The light grey histogram arises from a readout laser Rabi frequency of $\Omega \approx 0.41\gamma$, where γ is the spontaneous emission rate. The dark grey histogram arises from $\Omega \approx 0.23\gamma$. An exponential decay with a time constant (t_{off}) of 6 ms (19 ms for the dark grey histogram) exhibits the dependence of the off statistics on the laser power, consistent with the bimodal distribution shown in Fig. 3b (red histogram). We model the expected dependence of the decay time constant t_{off} as

$$\frac{1}{t_{\mathrm{off}}} = \frac{1}{t_{0\to1}} + \frac{\gamma_{\mathrm{sf}}\Omega^2}{4\Delta^2+\gamma^2+2\Omega^2} \qquad (1)$$

where Δ denotes the spectral detuning between the readout laser and the 0-to-$T_{+3/2}$ transition, γ_{sf} is the rate of optically induced spin-flips from states 0 to 1 and $t_{0\to1}$ is the natural spin relaxation time from state 0 to 1. The solid black circles in Fig. 3d are the t_{off} values extracted from the off-duration histograms as a function of Rabi frequency. The solid black curve is a fit to the data when $t_{0\to1}$ is 140 ms, while the upper (lower) boundary of the shaded region is obtained when $t_{0\to1}$ is fixed to 1 s (50 ms). The values for γ, γ_{sf} and Δ are $2\pi \times 250$ MHz, $2\pi \times 0.49$ MHz and $2\pi \times 8$ GHz as obtained by independent measurements (see Supplementary Information). Our operation regime prevents a more accurate determination of $t_{0\to1}$ in these experiments.

Each time bin in the observation of intermittent RF is also a single-shot measurement attempt on the host QD electron spin state. Figure 4a presents a 400-ms selection from the 1,200-s time trace of RF photocounts used to quantify the fidelity of our measurement. Each time bin is 2 ms and the horizontal dashed black line, determined by the intersection of the two distributions in Fig. 4b, indicates the threshold value of 17.5 RF photocounts—counts greater than 17.5 are assigned 1, and those less than 17.5 are assigned 0. The fidelity is evaluated as $1 - p_1e_1 - p_0e_0$, where p_1 is the probability of finding the electron in state 1 and e_1 is the error in assigning state 1, and p_0 is the probability of finding the electron in state 0 and e_0 is the error in assigning state 0. Two main sources contribute to e_1 and e_0. We use the RF photocounts histogram (inset to Fig. 4b) to determine one source of error (denoted $e_1^{\mathrm{n}}/e_0^{\mathrm{n}}$) by fitting each mode of the distribution independently to extract distributions that correspond to 1 and 0, assuming equal probability for the spin to be 1 or 0 before a measurement. The extracted RF photocount histograms for 1 and 0 are plotted in Fig. 4b. The area under the 1-distribution below the threshold contributes less than 10^{-3} to the value of e_1 and correspondingly the area under the 0-distribution above the threshold contributes less than 10^{-3} to the value of e_0. A second source of error is the probability that during the course of a single measurement time bin the host QD spin flips from 0 to 1 (or 1 to 0) and is incorrectly assigned to state 1 (or 0); we denote this error e_1^{d} (or e_0^{d}). The spin flips from 0 to 1 as a result of readout laser optical pumping via the detuned 0-to-$T_{+3/2}$ transition. To evaluate e_0^{d}, we take half the time bin size (1 ms) and divide it by the decay time constant t_{off} (14.9 ms), thus finding $e_0^{\mathrm{d}} = 0.07$. Likewise, if the spin flips from 1 to 0 by dynamics not induced by the laser a similar analysis (estimating $t_{1\to0} = 100$ ms) results in $e_1^{\mathrm{d}} = 0.01$ (see Supplementary Information). The overall estimated fidelity of 96% depends on the experimental configuration and we could reduce e_1^{d} and e_0^{d} at the

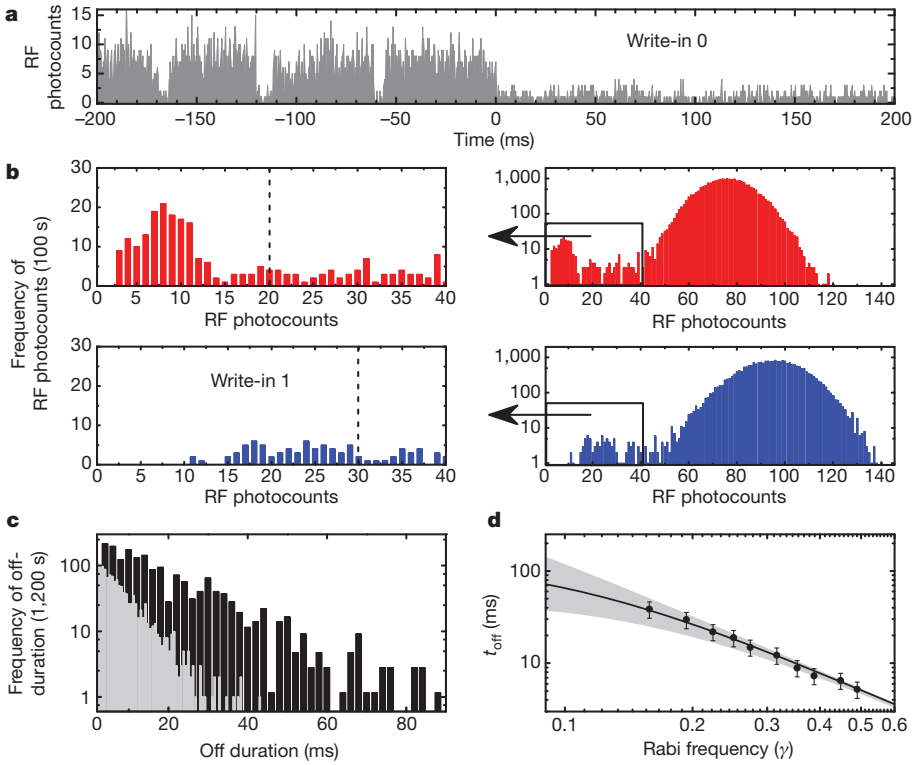

Figure 3 | Measurement of spin quantum jumps via intermittent resonance fluorescence. **a**, Time-resolved resonance fluorescence from the 1-to-$T_{+1/2}$ transition at a magnetic field of 2.3 T. The time bin for each data point is 250 μs. For negative times the readout laser alone drives the 1-to-$T_{+1/2}$ transition, whereas for positive times the write-in laser is turned on to prepare state 0. The signal is suppressed in the presence of the write-in laser. **b**, Top right panel, histogram of the frequency of RF photocounts for 100 s of RF data with time bins of 4 ms when the readout laser drives the 1-to-$T_{+1/2}$ transition. Top left panel, the region bounded by the black rectangle in the top right panel. The vertical dashed black line indicates the threshold value below which all RF photocounts are labelled 0. Bottom right panel, frequency of RF photocounts for 100 s of RF data with time bins of 4 ms when the readout laser drives the 1-to-$T_{+1/2}$ transition and the write-in laser prepares spin state 1 continuously. Bottom left panel, the region bounded by the black rectangle in the bottom right panel. The vertical dashed black line indicates the threshold value below which all RF photocounts are labelled 0. The quality of the RF signal relies strongly on the ability to suppress the laser-induced background. Although we achieve $\sim 10^5$ suppression for the single laser experiments, introduction of the second (write-in) laser introduces a small but finite background level of ~19 RF photocounts per bin on average for the histogram in the bottom panels. Hence the histogram is shifted by this rate, but the statistics of the RF photocounts are unaffected. **c**, A plot of the frequency of off-durations when the readout laser drives the 1-to-$T_{+1/2}$ transition with Rabi frequency values of $\Omega \approx 0.41\,\gamma$ (light grey histogram) and $\Omega \approx 0.23\,\gamma$ (dark grey histogram) where $\gamma = 2\pi \times 250$ MHz is the spontaneous emission rate. **d**, A plot of the characteristic decay time constant t_{off} from the off-duration histograms as a function of the readout laser Rabi frequency with $t_{0\to1}$ as the fit parameter. The solid black curve is a best-fit plot of equation (1) with $\gamma = 2\pi \times 250$ MHz, $\gamma_{sf} = 2\pi \times 0.49$ MHz, and $\Delta = 2\pi \times 8$ GHz for $t_{0\to1} = 140$ ms. The upper boundary of the shaded region is for $t_{0\to1}$ of 1 s and the lower boundary is for $t_{0\to1}$ of 50 ms. The error bars denote one standard deviation.

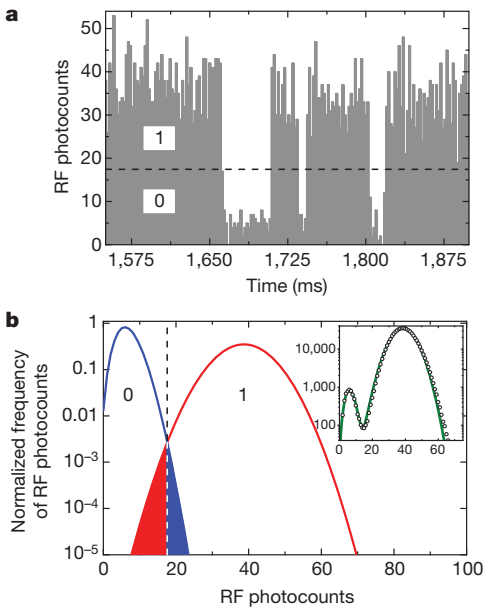

expense of increasing e_1^n and e_0^n by decreasing the measurement time bin.

The error e_0^d is a measure of our readout technique's invasiveness and an ideal non-demolition measurement would have no contribution from this type of error. A natural way to reduce e_0^d, and potentially realize a non-demolition measurement, is to increase the spectral separation between $T_{+1/2}$ and the other excited states, further suppressing laser-induced spin dynamics. A comprehensive study is necessary to identify the optimum point of operation for our readout technique. Nevertheless, the quality of the RF signal reported

Figure 4 | Measurement fidelity. **a**, An exemplary 400-ms time slice of the 1-to-$T_{+1/2}$ transition RF photocounts from the 1,200 s of data used for the analysis. The time bin per data point is 2 ms. The horizontal dashed black line indicates the 0/1 threshold value of 17.5 RF photocounts. **b**, The blue curve is the normalized 0 distribution of the frequency of RF photocounts and the red curve is the normalized 1 distribution. The red shaded area below the threshold (vertical dashed line) contributes to the error e_1 in assigning state 1 and the blue shaded area above the threshold contributes to the error e_0 in assigning state 0. The inset shows a histogram of the frequency of RF photocounts (black open circles) for 1,200 s of data. The green curve is the fit to the data using broadened Poissonian distributions for the 1 and 0 histograms (see Supplementary Information).

here is sufficient to enable a reliable single-shot state measurement at the end of a quantum operation.

METHODS SUMMARY

The InAs/GaAs QD molecules studied here were grown by molecular beam epitaxy and embedded in a Schottky diode heterostructure[13–15]. The host QD layer is 30 nm above the n^+ layer and the wetting layers of each QD are separated by 13 nm. The applied gate voltage dictates the electron occupancy of each QD via a nearby electron reservoir and tunes the relative energy separation between the electronic states of the two QDs. The sample is located in a magneto-optical bath cryostat and cooled to 4.2 K. A GaAs solid immersion lens is used to improve both the laser focusing and fluorescence collection of the fibre confocal microscope. All measurements use tuneable single-mode diode lasers with 1.2 MHz frequency stabilization and 0.5% power stabilization. When the laser is tuned to a transition, resonant scattering from the QD molecule is collected and directed to a single photon counting detector. By registering the RF photocounts we can achieve a signal-to-noise ratio of 1 for 30-μs measurement time bins[25], which results in a measurement time resolution that allows us to resolve the resonance fluorescence intermittency induced by changes in the QD molecule electron spin orientation. To suppress the background laser we operate the microscope in a dark-field configuration by placing a linear polarizer in the collection arm, perpendicular to the incoming polarization, thus providing extinction greater than 10^5. For the experiments in which a second laser is used to drive the write-in transitions, a spectral filter with 1-nm bandwidth is used to reduce the background caused by the second laser.

Received 23 March; accepted 15 July 2010.

1. Nielsen, M. A. & Chuang, I. L. *Quantum Computation and Quantum Information* (Cambridge University Press, 2000).
2. Hanson, R. & Awschalom, D. D. Coherent manipulation of single spins in semiconductors. *Nature* **453,** 1043–1049 (2008).
3. Imamoglu, A. *et al.* Quantum information processing using quantum dot spins and cavity QED. *Phys. Rev. Lett.* **83,** 4204–4207 (1999).
4. Atatüre, M. *et al.* Quantum-dot spin-state preparation with near-unit fidelity. *Science* **312,** 551–553 (2006).
5. Gerardot, B. D. *et al.* Optical pumping of a single hole spin in a quantum dot. *Nature* **451,** 441–443 (2008).
6. Wu, Y. *et al.* Selective optical control of electron spin coherence in singly charged GaAs-$Al_{0.3}Ga_{0.7}As$ quantum dots. *Phys. Rev. Lett.* **96,** 097402 (2007).
7. Berezovsky, J., Mikkelson, M. H., Stoltz, N. G., Coldren, L. A. & Awschalom, D. D. Picosecond coherent optical manipulation of a single electron spin in a quantum dot. *Science* **320,** 349–352 (2008).
8. Press, D., Ladd, T. D., Zhang, B. & Yamamoto, Y. Complete quantum control of a single quantum dot spin using ultrafast optical pulses. *Nature* **456,** 218–221 (2008).
9. Kroutvar, M. *et al.* Optically programmable electron spin memory using semiconductor quantum dots. *Nature* **432,** 81–84 (2004).
10. Berezovsky, J. *et al.* Nondestructive optical measurements of a single electron spin in a quantum dot. *Science* **314,** 1916–1920 (2006).
11. Atatüre, M., Dreiser, J., Badolato, A. & Imamoglu, A. Observation of Faraday rotation from a single confined spin. *Nature Phys.* **3,** 101–106 (2007).
12. Vamivakas, A. N., Zhao, Y., Lu, C.-Y. & Atatüre, M. Spin-resolved quantum dot resonance fluorescence. *Nature Phys.* **5,** 198–202 (2009).
13. Krenner, H. J. *et al.* Direct observation of controlled coupling in an individual quantum dot molecule. *Phys. Rev. Lett.* **94,** 057402 (2005).
14. Ortner, G. *et al.* Control of vertically coupled InGaAs/GaAs quantum dots with electric fields. *Phys. Rev. Lett.* **94,** 157401 (2005).
15. Stinaff, E. A. *et al.* Optical signature of coupled quantum dots. *Science* **311,** 636–639 (2006).
16. Flagg, E. B. *et al.* Resonantly driven coherent oscillations in a solid-state quantum emitter. *Nature Phys.* **5,** 203–207 (2009).
17. Dehmelt, H. G. Proposed 10^{14} Dv < v laser fluorescence spectroscopy on Tl+ mono-ion oscillator II (spontaneous quantum jumps). *Bull. Am. Phys. Soc.* **20,** 60 (1975).
18. Nagourney, W., Sandberg, J. & Dehmelt, H. Shelved optical electron amplifier: observation of quantum jumps. *Phys. Rev. Lett.* **56,** 2797–2799 (1986).
19. Sauter, T., Neuhauser, W., Blatt, R. & Toschek, P. E. Observation of quantum jumps. *Phys. Rev. Lett.* **57,** 1696–1698 (1986).
20. Bergquist, J. C., Hulet, R. G., Itano, W. M. & Wineland, D. J. Observation of quantum jumps in a single atom. *Phys. Rev. Lett.* **57,** 1699–1702 (1986).
21. Basch, Th, Kummer, S. & Bruchle, C. Direct spectroscopic observation of quantum jumps of a single molecule. *Nature* **373,** 132–134 (1995).
22. Leibfried, D., Blatt, R., Monroe, C. & Wineland, D. Quantum dynamics of single trapped ions. *Rev. Mod. Phys.* **75,** 281–324 (2003).
23. Imamoglu, A. Quantum computation using quantum dot spins and microcavities. *Fortschr. Phys.* **48,** 987–997 (2000).
24. Pazy, E., Calarco, T. & Zoller, P. Spin state readout by quantum jump technique: for the purpose of quantum computing. *IEEE Trans. NanoTechnol.* **3,** 10–16 (2004).
25. Lu, C.-Y. *et al.* Direct measurement of spin dynamics in InAs/GaAs quantum dots using time-revolved resonance fluorescence. *Phys. Rev. B* **81,** 035332 (2010).
26. Yilmaz, S. T., Fallahi, P. & Imamoglu, A. Quantum-dot-spin single-photon interface. *Phys. Rev. Lett.* **105,** 033601 (2010).
27. Kim, D. *et al.* Optical spin initialization and non-destructive measurement in a quantum dot molecule. *Phys. Rev. Lett.* **101,** 236804 (2008).
28. Fält, S. *et al.* Strong electron-hole exchange in coherently coupled quantum dots. *Phys. Rev. Lett.* **100,** 106401 (2008).
29. Robledo, L. *et al.* Conditional dynamics of interacting quantum dots. *Science* **320,** 772–775 (2008).
30. Doty, M. F. *et al.* Hole-spin mixing in InAs quantum dot molecules. *Phys. Rev. B* **81,** 035308 (2010).

Supplementary Information is linked to the online version of the paper at www.nature.com/nature.

Acknowledgements This work was supported by grants and funds from the University of Cambridge, EPSRC Science and Innovation Awards, the QIPIRC and EPSRC grant number EP/ G000883/1. Y.Z. is supported by the A. v. Humboldt Foundation and LGFG. We thank A. Imamoglu, X. Marie, T. Amand, D. Gammon and D. Steel for discussions.

Author Contributions A.N.V., C.-Y.L., C.M., Y.Z. and M.A. designed and performed the experiments, and conducted the analysis. S.F. and A.B. contributed to the growth and fabrication of the samples. All authors contributed to writing the paper.

Author Information Reprints and permissions information is available at www.nature.com/reprints. The authors declare no competing financial interests. Readers are welcome to comment on the online version of this article at www.nature.com/nature. Correspondence and requests for materials should be addressed to M.A. (ma424@cam.ac.uk) and A.N.V. (anv21@cam.ac.uk).